A Systematic Approach to Modeling Complex Magnetic Devices Using SPICE: Application to Variable Inductors

J. Marcos Alonso, *Senior Member, IEEE*, Gilberto Martínez, Marina Perdigão, *Member, IEEE*, Marcelo Rafael Cosetin, and Ricardo N. do Prado, *Member, IEEE*

***Abstract*—In this paper, a methodology to develop SPICE-based models of complex magnetic devices is presented. The proposed methodology is based on a reluctance equivalent circuit, which allows the user to study both the magnetic and electric behavior of the structure under any operating conditions. The different elements required to implement the reluctance model, namely, constant reluctances, variable reluctances, and windings, are implemented using SPICE behavioral modeling. These elements can thus be used to build a complete model for any magnetic device. The modeling process is illustrated with a particular example for a variable inductor. Simulations and experimental results are presented and compared to evaluate the accuracy and usefulness of the proposed modeling procedure.**

***Index Terms*—Magnetic devices, modeling, SPICE behavioral modeling, variable inductor (VI).**

I. Introduction

MODELING magnetic devices, such as inductors and transformers, has been a particularly important topic in power electronics. The great advances achieved in the last decades in the power electronics area in terms of miniaturization, efficiency improvement, and reliability, would have been impossible without new magnetic materials, devices, and modeling techniques. Understanding the real behavior of magnetic devices is a key issue to improve its performance, and that of the whole power electronics converter. Additionally, in today's power electronics applications, more complex magnetic structures are being employed, such as variable inductors (VIs) and transformers, saturable inductors and transformers, integrated magnetics, etc. [1]–[11].

Manuscript received March 10, 2016; accepted May 11, 2016. Date of publication May 24, 2016; date of current version June 24, 2016. This work was supported by the Spain National Government and Asturias Regional Government under research Grants ENE2013-41491-R and GRUPIN14-076, respectively.

J. Marcos Alonso is with the Department of Electrical Engineering, University of Oviedo, Oviedo 33003, Spain.

G. Martínez is with the Department of Electrical Engineering, University of Oviedo, Oviedo 33003, Spain, and also with Continental Automotive R&D; ID HMI Hardware Development Department, 45601-GDL, Jalisco, México .

M. Perdigão is with Instituto de Telecomunicações, University of Coimbra, Coimbra 3000-370, Portugal. He is also with Instituto Superior de Engenharia de Coimbra, Coimbra 3030-199, Portugal.

M. R. Cosetin and R. N. do Prado are with the Group of Intelligence in Lighting, Federal University of Santa Maria, Santa Maria 97105-900, Brazil.

This paper has supplementary downloadable multimedia material available at http://ieeexplore.ieee.org provided by the authors. The material is 48 KB in size.

Color versions of one or more of the figures in this paper are available online at http://ieeexplore.ieee.org.

Digital Object Identifier 10.1109/TPEL.2016.2571845

One of the more accurate and painless ways to study the behavior of magnetic structures is by using computer simulations. Basically, there are two methods to address this task: 1) finite elements analysis (FEA) and 2) SPICE-based behavioral models.

Surely, FEA provides the best accuracy, especially when using three-dimensional (3-D) models. However, it takes a considerable time to develop a 3-D model of a magnetic device. Moreover, the simulation time using FEA results very long; it can take many hours or even days to obtain the final results. Convergence problems may arise, breaking the simulation and wasting many hours of time. Any change or improvement in the model means a new simulation, making the analysis process quite painful and strenuous. On the other hand, computer simulation based on SPICE-like models results much more friendly; simulations can be done in seconds or minutes at the most, and they can easily be used within more complex electrical circuits or power converters. Of course, accuracy is lower than using FEA, nonetheless good enough for many applications.

In this paper, a SPICE-based model for computer simulation of any magnetic structure is presented. The proposed model is inspired on several models previously presented in the literature [12]–[17], which employed a reluctance or permeance equivalent circuit to simulate both the electrical and magnetic behavior of the magnetic structure. Particularly interesting is the methodology used in PSIM simulator [17]. However, the authors have found it too closed to allow the users to attain full benefit from it. This paper explores a similar methodology based on a reluctance model in which the reluctances depend on the magnetic flux level. A variable magnetic permeability, which is derived from the B–$HB - H$ curve of the magnetic material, is used to model the change of the reluctance. In this way, the different elements present in any magnetic structure, such as variable reluctances, air gaps, constant reluctances, and windings, will be modeled separately. Thus, they can be used to build an equivalent circuit of any magnetic structure. The model can be employed under any operating conditions, including dc and ac operation in any winding. In addition, the model will be able to provide electric and magnetic outcomes as voltage, current, magnetic flux, magnetic flux density, inductance, and so forth.

The original motivation to develop this study has been the investigation of the behavior of both saturable and controllable inductors and transformers. These devices have been studied and employed in power electronics applications for many years now with encouraging results [1]–[8], [12]–[26]. Particularly, controllable (variable) inductors are complex magnetic devices

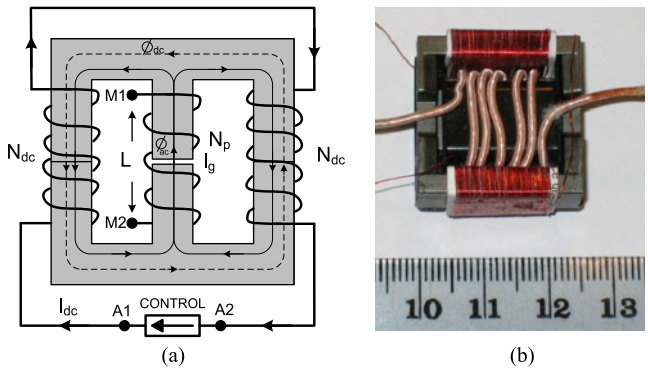

Fig. 1. Physical structure of a VI implemented in an EE core.

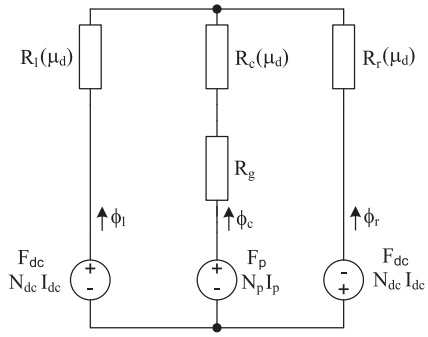

Fig. 2. Reluctance equivalent circuit of the VI shown in Fig. 1.

that deal with several windings under ac and dc superposed operation. In these devices, the reluctance of some sections of the magnetic material experiences a great variation owing to the dc component of the magnetic flux, even though the ac component remains under the saturation level. This makes a conventional analysis of these devices very laborious, while by using computer simulations it can be carried out very easily. Also, computer simulations allow the designer to change core geometry, magnetic properties, number of turns, air gap length, current, and voltage levels, etc., making design and redesign processes extremely straightforward.

In Section II, a review of the VI structure that will be used as a modeling example is carried out. Section III presents the modeling of the different elements of the reluctance equivalent model of a magnetic device. Section IV shows the implementation of the VI SPICE model using the proposed methodology. Section V presents simulation and experimental results. Finally, the conclusions of this study are provided in Section VI. This paper is a revised version of [27], in which several corrections and improvements have been made.

II. Review of the Selected VI Structure

In this paper, the VI structure based on a double E core, as shown in Fig. 1, will be employed as an example to illustrate the use of the proposed modeling technique.

The detailed operation of this device has been presented in previous literature [5] [7] [8]. A summary of its structure and operation can be made as follows. A double-E core with a gapped center arm is used, while no gap is present in the left and right arms. The main coil is wound on the center arm with a given number of turns N_p, which will implement the main inductor. Two auxiliary windings are placed on the left and right arms of the core, with an equal number of turns N_{dc} and with reversed polarity, so that the ac voltages generated across them tend to cancel each other when connected in series. Actually, as demonstrated in [13], a full cancellation is not possible due to the nonlinear behavior of the magnetic material *B–H* curve around the saturation knee. This is one of the aspects that would be very difficult to tackle by an analytical study. However, it is possible to deal with this issue quite straightforwardly by computer simulation.

In the VI structure, a dc current is injected through the auxiliary windings. This generates a dc flux bias that circulates mainly through the outer part of the core, because the center arm is gapped and exhibits a much higher reluctance. On the other hand, the ac flux circulating through the main winding splits into the outer arms, as shown in Fig. 1(a). The dc flux is used to bias the operating point of the magnetic material within the *B–H* curve, thus modifying the reluctances and changing the value of the inductance as seen from the main winding terminals.

This device can be modeled by using the reluctance circuit shown in Fig. 2. In this circuit, $\Re_c$, $\Re_l$, and $\Re_r$ represent the reluctances of the center, left, and right arms, respectively, and, in a general case, their values depend on the dc operating point of the magnetic material, and can therefore be expressed as a function of the material magnetic permeability. $\Re_g$ represents the air gap reluctance and can be assumed as a constant.

The other components in the circuit are the voltage sources F_{dc} and F_p, which represent the magnetomotive forces (MMF) created by the auxiliary and main windings, respectively, which are given by the turns by current product. Next section will present how the different elements of the reluctance model can be implemented following the methodology presented in this study.

III. Basic Elements of the Reluctance Equivalent Circuit

The basic elements of a reluctance equivalent circuit are three: 1) constant reluctances, which model an air gap or any other nonferromagnetic material used in the core structure; 2) variable reluctances, used to model the nonlinear behavior of the magnetic material of the core; and 3) windings, which model the interaction between the electric and magnetic quantities involved in the behavior of any magnetic device. Once these elements are independently modeled for computer simulation, they can be used to implement any magnetic structure model, disregarding its complexity.

A. Constant Reluctance Model

A constant reluctance is used to model the behavior of a nonferromagnetic section of the magnetic device. In the reluctance equivalent circuit, a constant reluctance is modeled by a resistor,

whose value is defined as

$$\Re_0 = \frac{l_0}{\mu_0 \, A_0 \nu} \tag{1}$$

where l_0, and A_0 are the length and section of the constant reluctance element, respectively, $\mu_0 = 4\pi 10^{-7}$ H/m is the permeability of free space, and ν is the fringing coefficient, which is equal to 1 when the fringing effect is disregarded. However, a value slightly higher than 1 will usually render a better accuracy. Note that reluctance units are H^{-1}.

B. Variable Reluctance Model

A variable reluctance models the nonlinear behavior of the magnetic material employed in the device. It can be expressed as

$$\Re_m (B) = \frac{l_m}{\mu_d (B) \, A_m} \tag{2}$$

where l_m, and A_m are the length and section of the variable reluctance element, respectively, and $\mu_d(B)$ is the absolute differential permeability of the material, expressed as a function of the magnetic flux density B.

As can be seen in (2), in this type of element, the reluctance is a function of the magnetic permeability of the material, which in turn depends on the dc operating point within the material *B–H* curve. Therefore, at this point, it is necessary to find a model for the *B–H* characteristic of the magnetic material, from which the permeability can be obtained.

In this study, after testing other possibilities, Brauer's model of the *B–H* curve has been selected [28]–[29]. This model defines the relationship between the magnetic field intensity H and the magnetic flux density B, by expressing H as a function of B as

$$H (B) = \left(k_1 e^{k_2 B^2} + k_3 \right) B \tag{3}$$

where k_1, k_2, and k_3 are the Brauer's model constants for each magnetic material.

For the sake of simplicity, the hysteresis effect is being neglected in this study, as it is usually done in most FEA software. From (3), it is very simple to obtain the differential permeability of the magnetic material by differentiation. The result is given in a closed form in (4). Also, note that (4) is valid for positive and negative values of B, because the $\mu_d(B)$ curve is symmetrical with respect to the vertical axis

$$\mu_d (B) = \frac{dB}{dH} = \left[k_1 \left(1 + 2 k_2 B^2 \right) e^{k_2 B^2} + k_3 \right]^{-1}. \tag{4}$$

As an example, which will also be used to test the proposed model against experimental measurements, the N87 material from TDK-EPCOS has been modeled [30]. Brauer's model coefficients were derived from the graphical information given by the manufacturer's datasheet [30], obtaining the *B–H* curve data points and using a mathematical software for curve-fitting. The resulting values are shown in Table I. Fig. 3 shows a comparison between manufacturer's datasheet information and Brauer's model, both for N87 material at 25°C. With this approximation,

TABLE I
BRAUER'S COEFFICIENTS FOR N87 MATERIAL AT 25ºC

Parameter	Value
k_1	$0.062\ \mathrm{A\,m^{-1}\,T^{-1}}$
k_2	$42.995\ \mathrm{T^{-2}}$
k_3	$302.904\ \mathrm{A\,m^{-1}\,T^{-1}}$

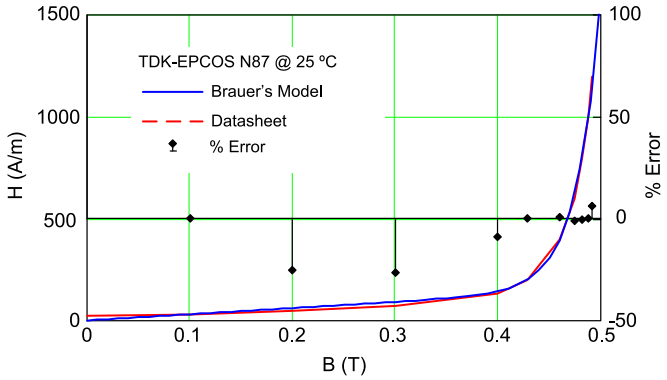

Fig. 3. *B–H* curve of N87 material at 25°C. Comparison between datasheet information and Brauer's model.

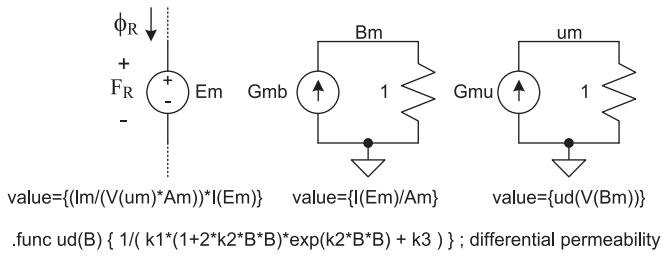

Fig. 4. Implementation of a variable reluctance in LTspice.

the maximum relative error was obtained at $B = 0.3$ T and was calculated as 26%.

Fig. 4 shows the implementation of the variable reluctance component in SPICE, particularly in LTspice, which is the software that has been selected in this study [31]. As can be seen in Fig. 4, a behavioral voltage source E_m is used to implement a resistive behavior that models the variable reluctance. The behavioral current source G_{mb} generates a current equal to the flux density in the magnetic element, which is transformed into a voltage at node B_m. The behavioral current source G_{mu} generates a current equal to the actual differential permeability of the magnetic material by implementing (4). Finally, the voltage at node u_m is used in the expression of E_m to define the component reluctance by using (2).

C. Winding Model

A winding model must represent the electrical and magnetic interaction within the magnetic device structure. Neglecting losses, the winding model can be expressed as follows:

$$\mathcal{F}_w (t) = N_w \cdot i_w (t) \tag{5}$$

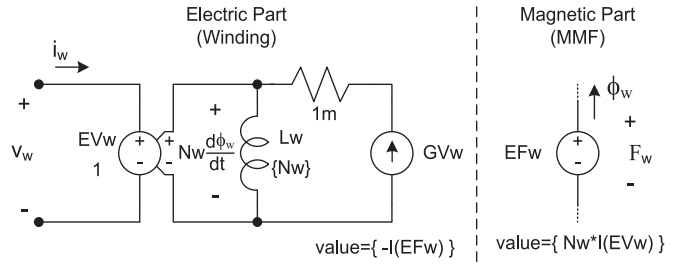

Fig. 5. Winding model implemented in LTspice.

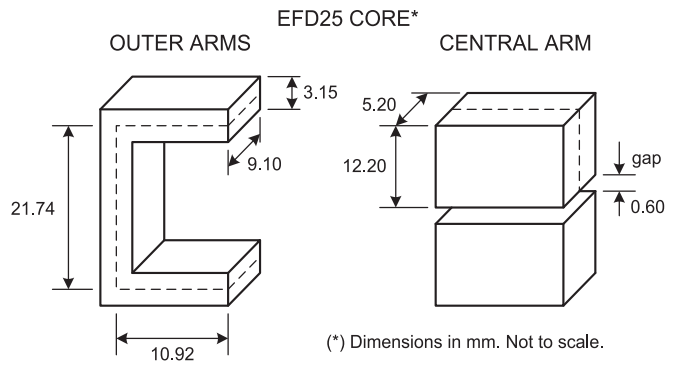

Fig. 6. EFD25 core dimensions [30].

$$v_w\ (t) = N_w\ \cdot \frac{d\emptyset_w\ (t)}{dt} = N_w\ A_w \frac{dB_w\ (t)}{dt} \tag{6}$$

where $\mathcal{F}_w$ is the MMF created by the winding inside the magnetic core, N_w is the winding number of turns, v_w and i_w are the winding voltage and current, $\emptyset_w$ and B_w are the magnetic flux and magnetic flux density in the core, respectively, and A_w is the area of the core.

Fig. 5 shows the SPICE implementation of the winding model. A voltage-dependent voltage source EV_w is used to implement the relationship between voltage and flux as given by (6). The behavioral voltage source EF_w is employed in the magnetic part of the model to generate the corresponding MMF according to (5). The behavioral current source GV_w generates a current equal to the magnetic flux, which is differentiated with respect to time by using the inductance L_w with a value equal to the number of turns of the winding (N_w) so that (6) can be implemented. The 1-mΩ resistance placed in series with GV_w is used to avoid convergence issues during simulation.

IV. Implementation of the VI Model

By using the three basic elements presented in the previous section, the reluctance equivalent circuit of any magnetic structure can be implemented for SPICE simulation. In this section, a model developed for the VI shown in Fig. 1 will be presented. This particular VI has been used in a previous work for the controlling of the output voltage in dc–dc resonant converters [20].

Fig. 6 illustrates the geometric diagram of the EFD25 core, which is used to calculate the average lengths and sections of the magnetic paths. Table II gathers the values of all the parameters related to the VI under study.

TABLE II
VI Data

Core material	N87 TDK-EPCOS	**Air gap length**	0.6 mm
Core type	EFD25	**Estimated fringing factor** (ν)	1.06
Expected inductance range	$1.2 - 4.5\mu$H	**Central arm average length** (lc)	24.4 mm
Main winding turns (N_p)	6	**Central arm section** (A_c)	59.3 mm^2
Intended operation regime	Sinusoidal, 500 kHz	**Outer arms average length** (l_1)	43.6 mm
Main winding peak current	6.0 A	**Outer arms section** (A_1)	28.7 mm^2
Bias windings turns (N_{dc})	65		

Fig. 7 illustrates the complete electrical diagram of the VI implemented in LTspice. As can be seen, it is divided into two main parts: magnetic part and electric part.

The magnetic part includes the reluctance model, where the variable reluctances $\Re_l$, $\Re_c$, and $\Re_r$ of Fig. 2 are implemented through the voltage sources E_5, E_3, and E_4, respectively. The magnetic flux density and permeability on each arm are calculated by current sources G_5, G_3 (central arm), G_8, G_6 (right arm), and G_{11}, G_9 (left arm). Reluctances R_{sl}, R_{sc}, and R_{sr} shown in Fig. 7 are used to measure the flux on each arm and to avoid voltage-loop issues during simulation. Their value of 1 H^{-1} is very small compared to the other series reluctances and therefore have no effect on the structure. Voltage source E_1 implements the magnetic part of the main winding of the VI, while voltage sources E_7 and E_6 implement the magnetic part of the left and right auxiliary windings, respectively.

The electric part of the model includes the implementation of the electric part of the three windings of the VI. Thus, sources E_2, G_1, and L_1 implement the behavior of the main winding, E_8, G_{12}, and L_2 correspond to the right auxiliary winding and E_9, G_{13}, and L_3 to the left auxiliary winding. Note that some additional small value resistors $(R_3,\ R_6,\ R_7,\ R_8,\ R_{13})$ are required to avoid voltage-loop and convergence issues.

The circuit shown in Fig. 7 can be employed to perform a dc transient simulation. Thus, the main winding is supplied with a 1-V dc voltage source with a 10-Ω series resistance. Auxiliary windings are supplied by using a dc current source with an output impedance of 100 kΩ. An important point that must be highlighted is that the auxiliary windings must be supplied with a dc source with a high output impedance, just as it is done in a real application. In this way, any interaction of the auxiliary source on the VI will be avoided.

The behavioral current source G_2 is used to calculate the inductance of the main winding by multiplying the flux of the main winding by its number of turns and dividing by its current.

The dc operating point simulation (.dc directive in SPICE) of the circuit shown in Fig. 7 will provide the steady-state values of all magnetic and electric variables of the VI, including the inductance value, given as a voltage at node L_SPICE.

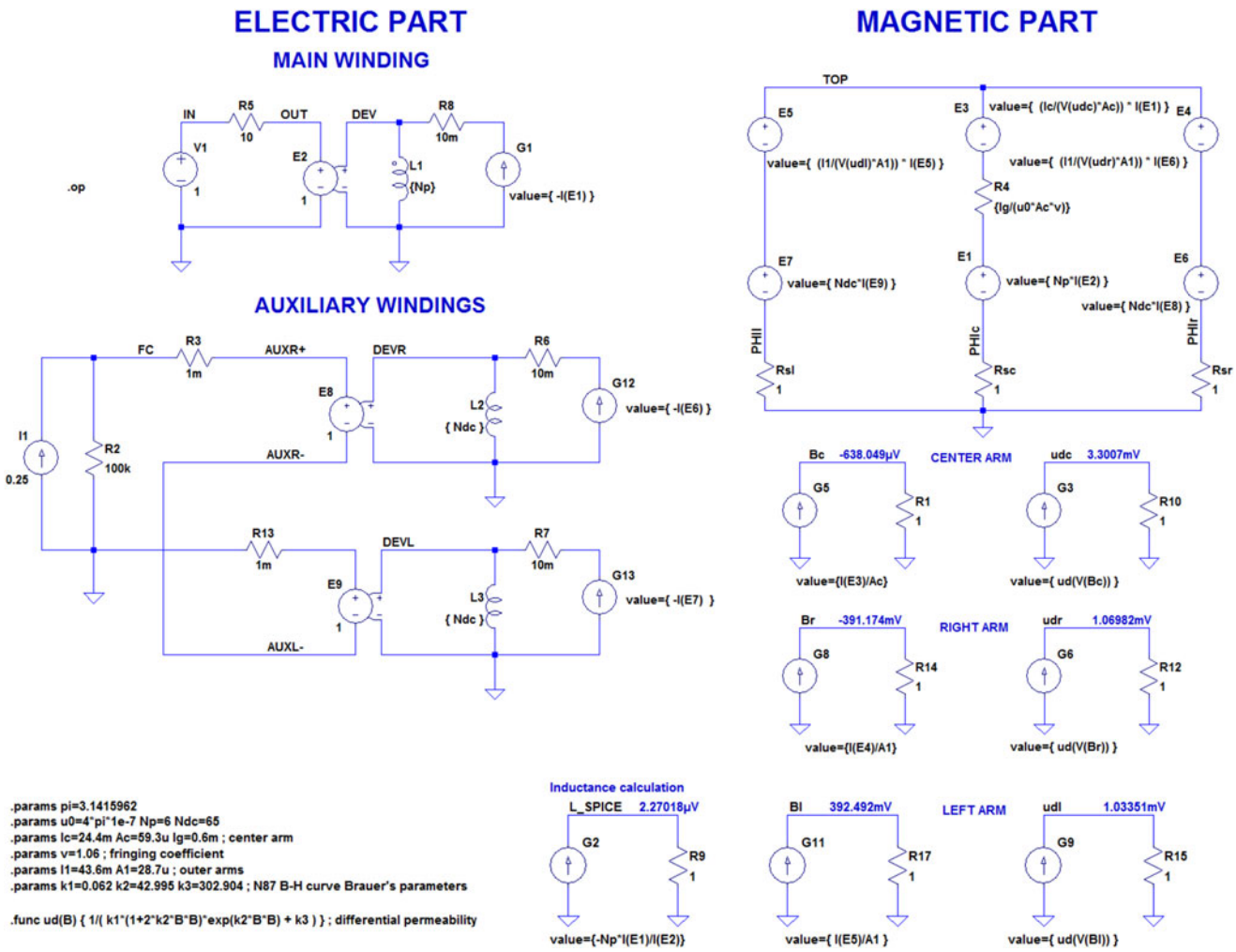

Fig. 7. Complete electrical model of the VI implemented in LTspice.

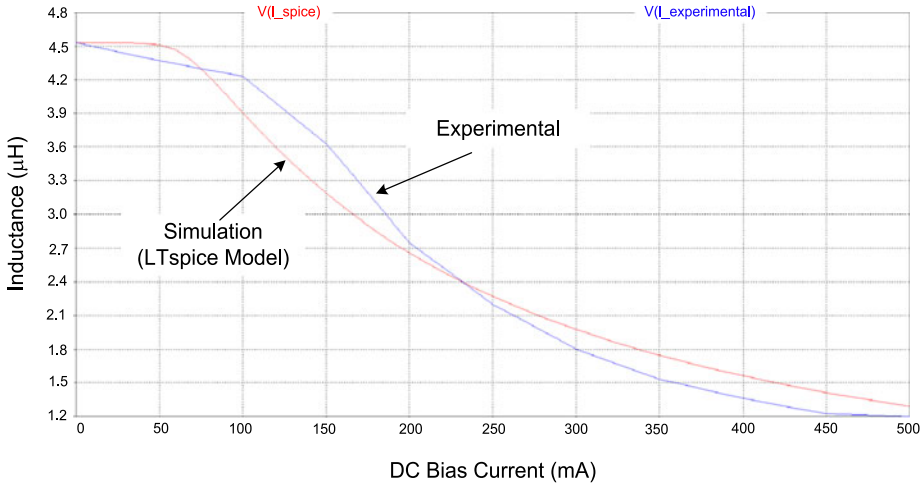

Fig. 8. Small-signal inductance of the VI. Comparison between simulation and experimental results.

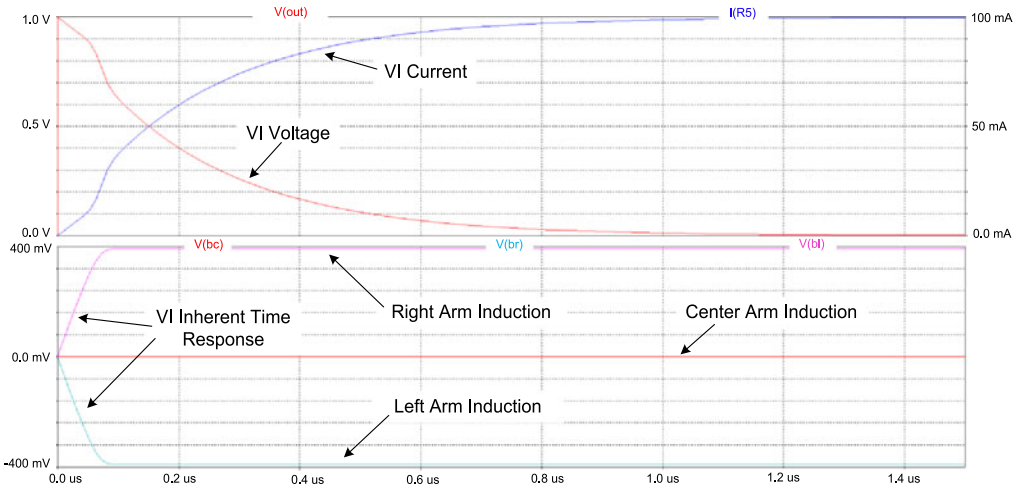

Fig. 9. Simulations results of the VI model under a dc start-up transient.

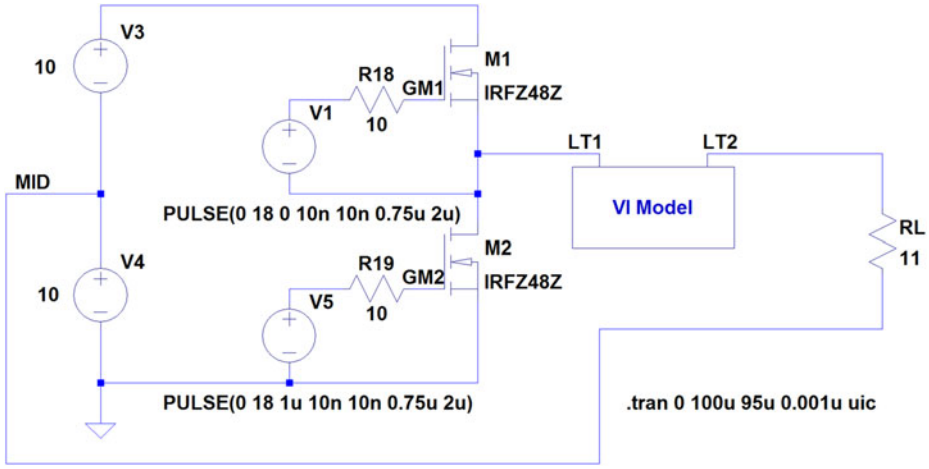

Fig. 10. Electric diagram for the simulation of an *L–R* inverter with VI. The VI is placed across terminals LT1 and LT2 according to the schematic shown in Fig. 7. Readers can refer to the active content for further details.

V. Simulation and Experimental Results

The first simulation carried out was a dc operating point (.dc) using the circuit shown in Fig. 7, in which a small current of 0.1 A is injected to the main winding to reach steady state, while the auxiliary windings carry a dc current of 0.25 A. Fig. 7 itself shows the simulation results by means of the voltage labels on each relevant node. As can be seen, the resulting inductance value is 2.27μH (voltage at node L_SPICE). The magnetic flux density at central, right, and left arms are obtained as voltage at nodes B_c, B_r, and B_l, giving –638.05 μ T, –391.17 mT, and 392.49 mT, respectively. Therefore, the central arm is operating with almost zero flux density (origin of the *B–H* curve), while the right and left arms are operated at a given dc flux density level owing to their biasing by the auxiliary windings, and in opposite direction. The small difference of flux density between left and right arms is due to the small flux level (0.638 mT) generated through the main winding, which adds to the left arm flux density, while subtracts from the right arm's.

The magnetic permeability of central, right, and left arms is obtained as voltages at nodes u_c, u_r, and u_l, respectively. The resulting values are 3.30, 1.070, and 1.033 mH/m, for central, right, and left arms, respectively. As expected, the permeability of the central arm is higher because of the lower flux density; the material of the central arm is operated around the origin of the *B–H* curve. On the other hand, the permeability of right and left arms is lower, because they operate at a much higher flux density level, within the knee of the *B–H* curve.

The above-presented simulation under dc operation can also be used to obtain the small-signal value of the VI inductance with very fast simulations. This can be done by performing a dc sweep analysis over the dc bias current source, shown as I_1 in Fig. 7. Following this procedure, Fig. 8 shows the simulation results in comparison with the experimental results obtained at the laboratory by using an impedance analyzer under small signal measurement of the inductance at a frequency of 1 kHz. Experimental results were added into the simulation for the sake of comparison by using a voltage-controlled source with a

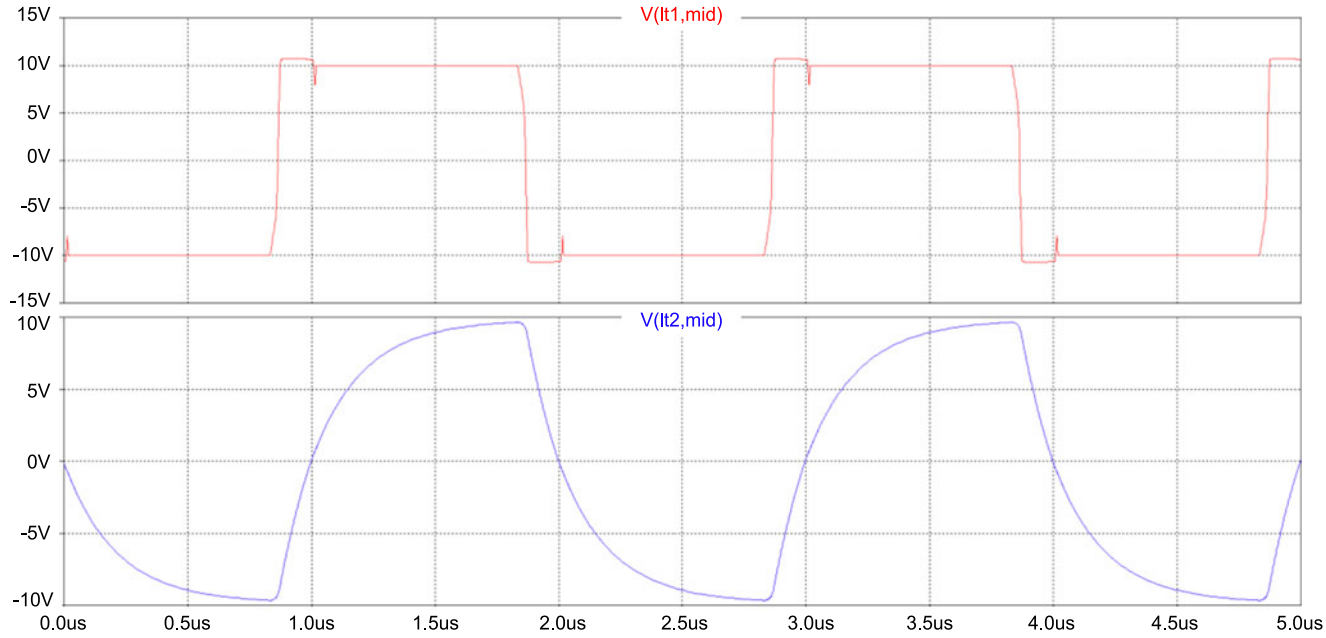

(a)

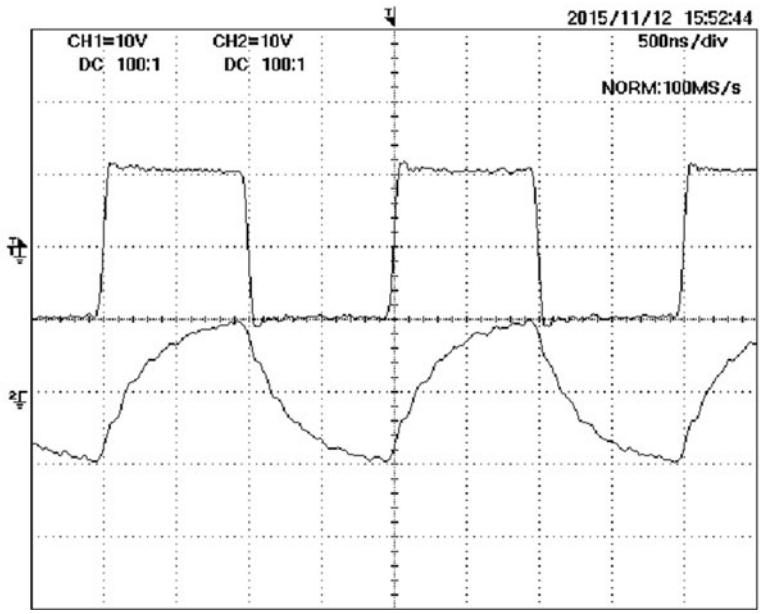

(b)

Fig. 11. Square voltage (top) and output voltage (bottom) of the circuit shown in Fig. 10: (a) simulation and (b) experimental. VI bias current 0.25 A.

look-up table (not shown in Fig. 7). Relative errors of –11% at 0.125-A bias current and +25% at 0.45-A bias current can be measured.

The difference between simulation and experimental results can be justified by three causes: 1) tolerances during the magnetic material fabrication, producing that the actual material *B–H* curve is not exactly the same as that given in the manufacturer's datasheet, 2) the error in the approximation of the *B–H* curve by the selected equation, in this case Brauer's model, 3) the effect of the leakage flux; the inclusion of a parallel reluctance to model, the leakage flux can render more approximated results. This effect will also be explored in future works [32] [33].

As an example, Fig. 9 shows the waveforms obtained from the same circuit shown in Fig. 7 when a transient simulation is performed. The inductor voltage and current, and the flux density inside the three arms of the structure are shown in this figure. As can be seen, it takes some time to the flux densities in right and left arms to reach their steady-state values, 50 ns approximately. This time is related to the dynamic response of the VI model. In the proposed model, this time is influenced by the output resistance of the current source that supplies the auxiliary

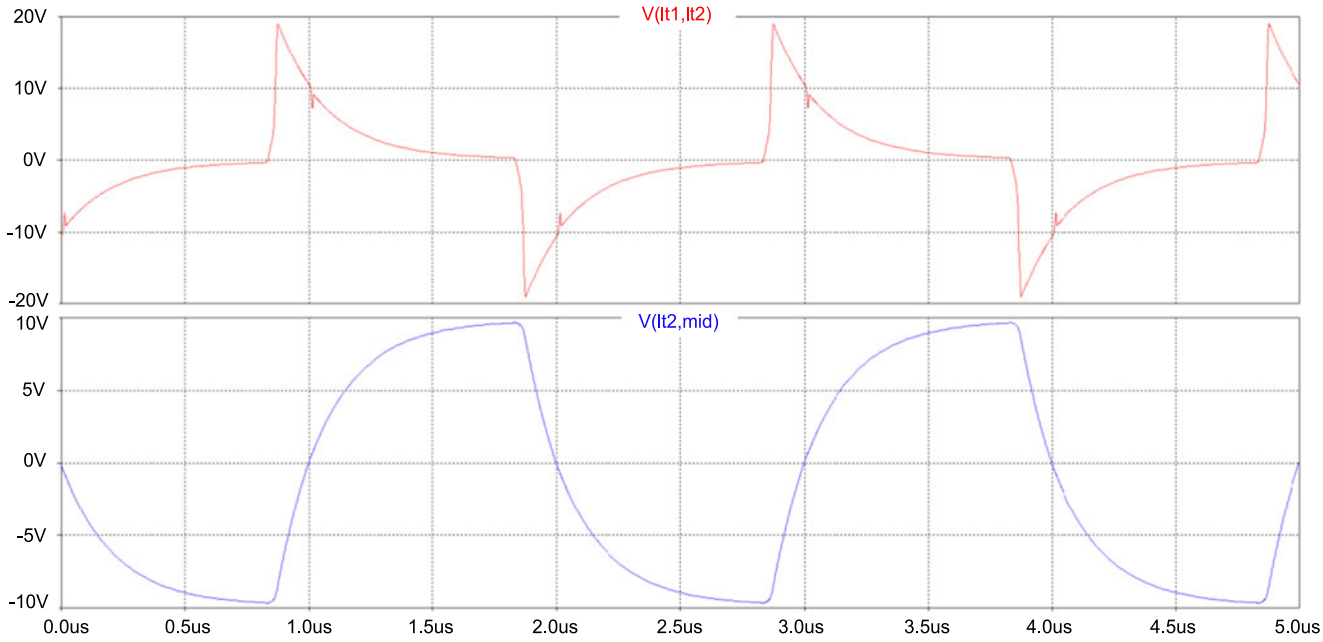

(a)

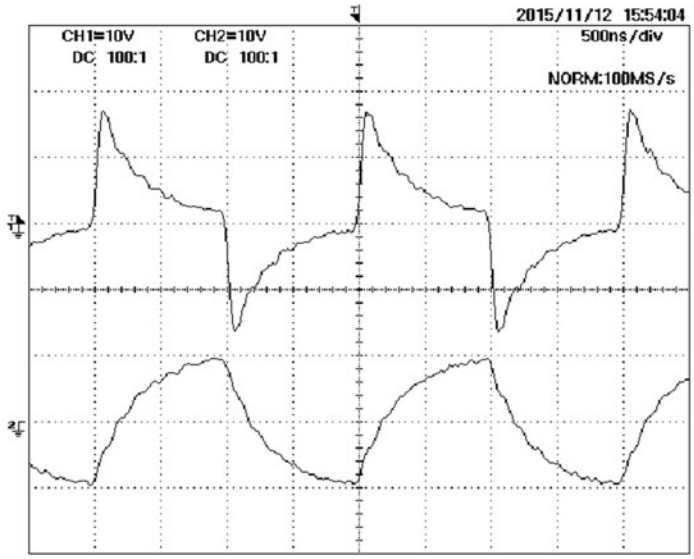

(b)

Fig. 12. VI voltage (top) and output voltage (bottom) of the circuit shown in Fig. 10: (a) simulation and (b) experimental. VI bias current 0.25 A.

winding and the equivalent inductance seen from the auxiliary winding. In the example under study, an output resistance of 100 kΩ has been selected in order to have a dynamic response fast enough so that it can be used up to frequencies of several hundreds of kilohertz. Nevertheless, this is a point that requires further investigation. In order to get more accurate results, the VI and its driving circuit should be dynamically modeled, theoretically or experimentally, and the time constant should be adjusted according to the obtained results. These issues will be addressed in future works [32] [33].

Fig. 10 illustrates the electrical diagram used for the simulation of a dc–ac converter with VI control. The converter has an input voltage of 20 V, applying a 10-V peak voltage square waveform to the L–$RL-R$ circuit. The switches are operated at 500 kHz with 200-ns dead time. The load resistance is 11Ω. In the following, simulation and experimental results corresponding to this circuit are presented.

Fig. 11 shows the simulation and experimental results corresponding to the square wave voltage and the output voltage across the load resistance for a VI bias current of 0.25 A. Fig. 12 illustrates the voltage across the VI and the output voltage for the same value of the VI bias current. As can be seen, simulation and experimental results match well.

Fig. 13 shows the simulation and experimental results corresponding to the VI bias windings. As can be seen, bias windings reflect voltages with peak values around 100 V. As expected, a

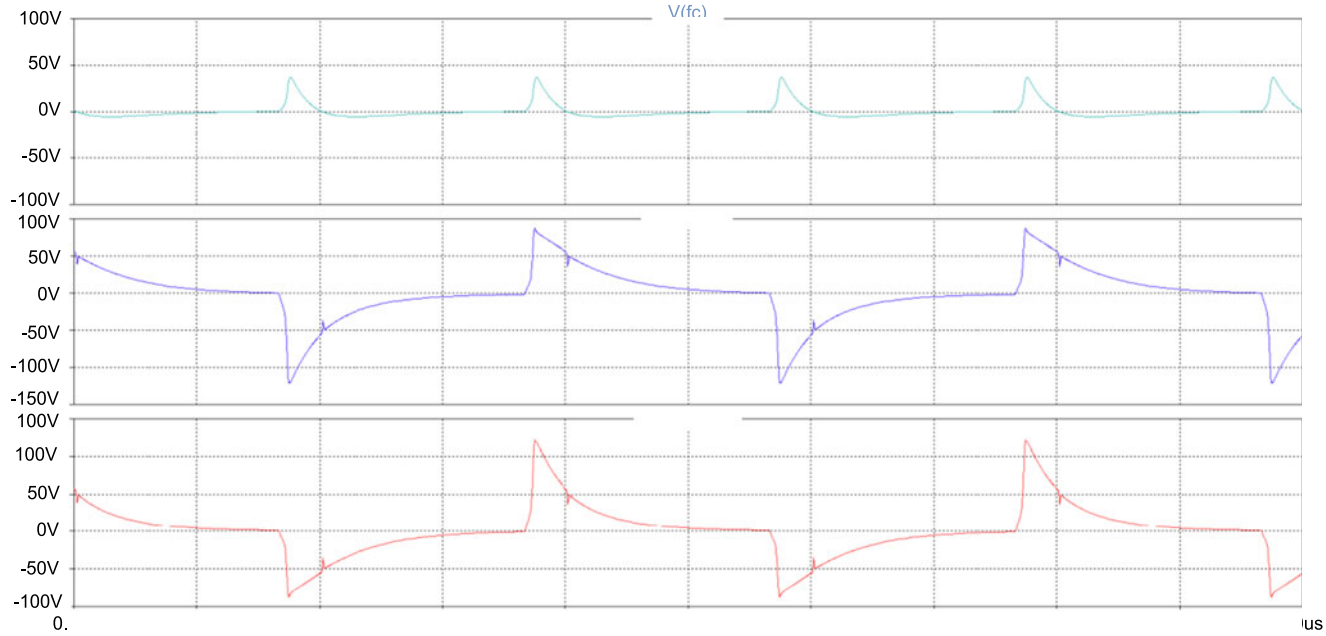

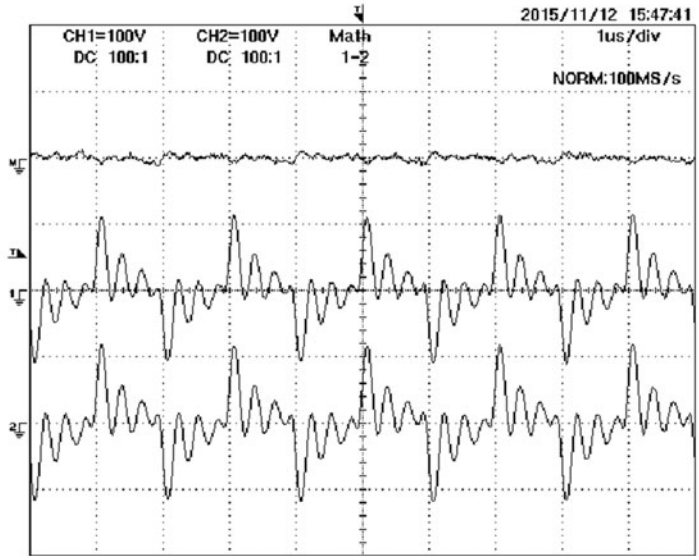

(b)

Fig. 13. Top: total voltage across VI bias windings. Middle: voltage across left bias winding. Bottom: voltage across right bias winding. All of them corresponding to the circuit shown in Fig. 10. (a) simulation and (b) experimental. VI bias current 0.25 A.

small difference can be seen comparing the voltages of left and right bias windings. As commented before, this difference is due to the nonlinear behavior of the magnetic material around the knee of the *B–H* curve [13]. However, the difference is higher in the simulation than in the experiments. This disagreement could be due to the response of the oscilloscope probe, which could not be able to follow so high *dv/dt*. Also, the high-voltage ripple superposed to the experimental waveform does not appear in the simulation. This ripple could also appear due to the effect of the oscilloscope voltage probe or other parasitic elements not considered by the model. The voltage probe used in these measurements was a differential voltage probe model 700924 from Yokowaga with 1:100 attenuation selected.

Fig. 14 shows the simulation results from the circuit in Fig. 10 corresponding to the instantaneous flux density in left, right, and center arms of the structure, and also to the instantaneous inductance of the VI. All of them are obtained from the corresponding nodes in the model. The VI bias current is 0.25 A. Experimental results are not available for these variables due to the difficulty of measuring dc levels of flux density inside a magnetic material. Nevertheless, the simulation results are in accordance with the expected ones.

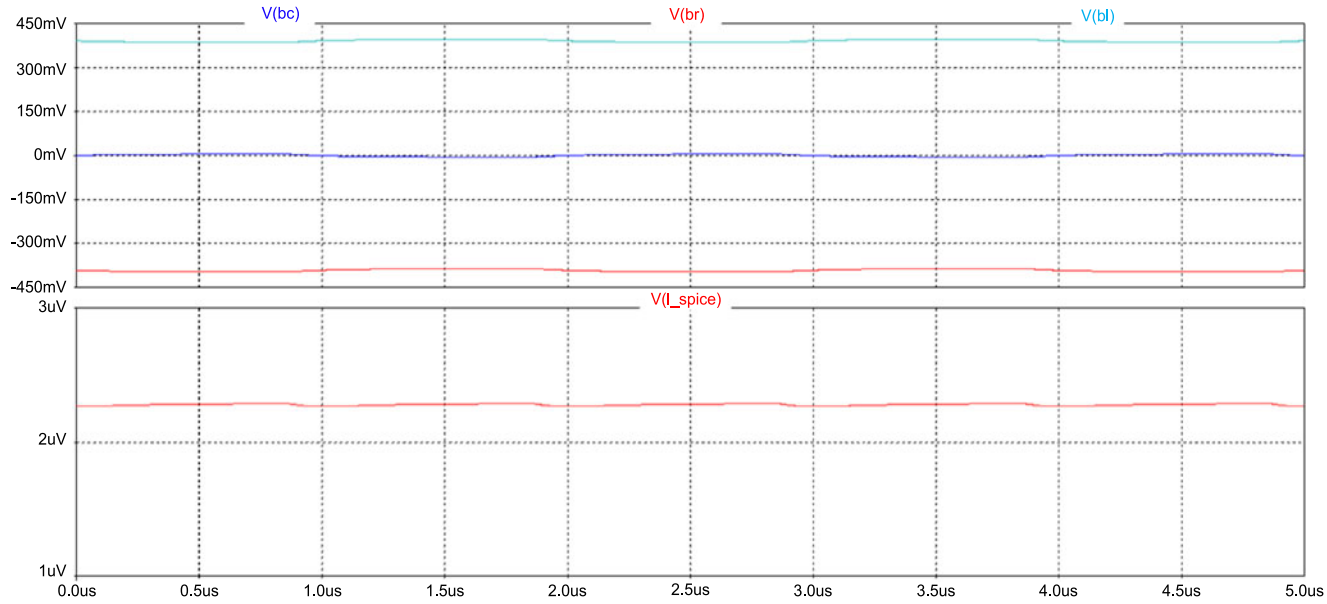

Fig. 14. Simulation results of the circuit in Fig. 10 with the VI bias current of 0.25 A. Top: flux density in each VI arm. Right arm (top), center arm (middle), and left arm (bot.). Scales: 200 mT/div. 500 ns/div. Bottom: inductance of the VI as obtained from the model. Scales: 1 μH/div, 500 ns/div.

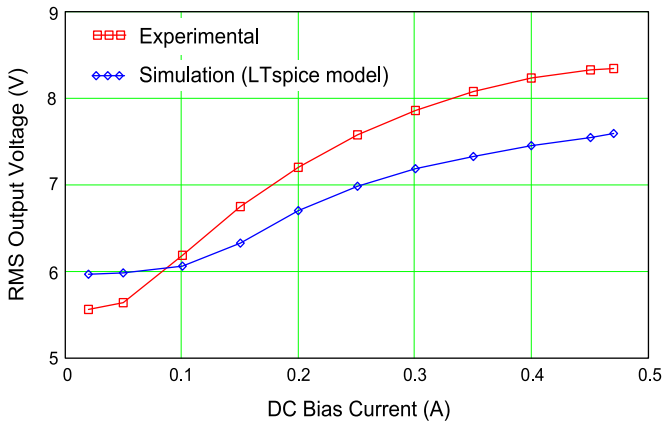

Fig. 15. Comparison between experimental and simulation results. RMS output voltage as a function of the VI dc bias current for the converter shown in Fig. 10.

Finally, in order to test the possibility of controlling the output voltage by means of the bias current on the VI, Fig. 15 presents the simulation and experimental results of the rms voltage in the load resistance of the circuit in Fig. 10 when varying the dc bias current of the VI. As can be seen, simulation and experimental results exhibit a similar curve. Again, the difference between simulation and experiments can be justified by the error in the modeling of the magnetic material *B–H* curve.

VI. Conclusion

This paper has presented a modeling technique for magnetic devices based on SPICE behavioral modeling. The three basic elements required for developing a reluctance-based equivalent circuit have been implemented in SPICE. These elements can easily be integrated in a SPICE library in order to simplify its use in circuit simulation [33]. It has been explained how by using these three elements any magnetic structure can be modeled and simulated providing magnetic, electric, and inductance results. Besides, the proposed modeling technique can be used under any operating conditions with good accuracy, because the nonlinear behavior of the magnetic material is taken into consideration. A modeling example of a VI with an EE structure has been presented and simulated, showing good approximation with experimental results. Simulation and experimental results for a VI-controlled dc–ac inverter have also been presented. The comparison between simulated and experimental results rendered good expectancies for the proposed modeling methodology.

Finally, it must be pointed out that the proposed methodology can also be implemented by using mathematical software packages, which could be used to solve the corresponding set of equations. The advantage of using a SPICE model resides in the fact that the model can easily be used to perform complete simulations including the power converter or other any electric or electronic circuit in which the VI is intended to operate.

References

[1] A. S. Kislovski, "Quasi-linear controllable inductor," *Proc. IEEE*, vol. 75, no. 2, pp. 267–269, Feb. 1987.
[2] A. S. Kislovski, "Linear variable inductor in dc current sensors utilized in telecom solar battery chargers," in *Proc. Int. Telecommun. Energy Conf.*, 1989, pp. 1–3.
[3] A. S. Kislovski, "Linear variable inductor (LVI) in single-phase off-line telecom rectifiers," in *Proc. IEEE Int. Telecommun. Energy Conf.*, 1995, pp. 93–98.
[4] D. L. Birx and L. L. Reginato, "Saturable inductor and transformer structures for magnetic pulse compression," U.S. Patent 4 928 020, 1990.
[5] D. Medini and S. Ben-Yaakov, "A current-controlled variable-inductor for high frequency resonant power circuits," in *Proc. Appl. Power Electron. Conf. Expo.*, Feb. 1994, vol. 1, pp. 219–225.
[6] W. H. Wölfle and W. G. Hurley, "Quasi-active power factor correction with a variable inductive filter: Theory, design and practice," *IEEE Trans. Power Electron.*, vol. 18, no. 1 pp. 248–255, Jan. 2003.

[7] J. M. Alonso, M. A. Dalla Costa, J. Cardesín, and J. Garcia, "Magnetic dimming of electronic ballasts," *Electron. Lett.*, vol. 41, no. 12, pp. 718–719, Jun. 2005.
[8] M. S. Perdigão, J. M. Alonso, D.G. Vaquero, and E. S. Saraiva, "Magnetically controlled electronic ballasts with isolated output: The variable transformer solution," *IEEE Trans. Ind. Electron.*, vol. 58, no. 9, pp. 4117–4129, Sep. 2011.
[9] M. Pahlevani, S. Eren, A. Bakhshai, and P. Jain, "A series–parallel current-driven full-bridge DC/DC converter," *IEEE Trans. Power Electron.*, vol. 31, no. 2, pp. 1275–1293, Feb. 2016.
[10] G. Gohil, L. Bede, R. Teodorescu, T. Kerekes, and F. Blaabjerg, "An integrated inductor for parallel interleaved three-phase voltage source converters," *IEEE Trans. Power Electron.*, vol. 31, no. 5, pp. 3400–3414, May 2016.
[11] H. Zhu, D. Zhang, Q. Liu, and Z. Zhou, "Three-Port DC/DC Converter with all ports current ripple cancellation using integrated magnetic technique," *IEEE Trans. Power Electron.*, vol. 31, no. 3, pp. 2174–2186, Mar. 2016.
[12] D. C. Hamill, "Gyrator-capacitor modeling: A better way of understanding magnetic components," in *Proc. Appl. Power Electron. Conf. Expo.*, 1994, vol. 1, pp. 326–332.
[13] E. Rozanov and S. Ben-Yaakov, "Analysis of current-controlled inductors by new SPICE behavioral model," *HAIT J. Sci. Eng. B*, vol. 2, no. 3–4, pp. 558–570, 2005.
[14] K. D. T. Ngo, "Subcircuit modeling of magnetic cores with hysteresis in PSpice," *IEEE Trans. Aerosp. Electron. Syst.*, vol. 38, no. 4, pp. 1425–1434, Oct. 2002.
[15] M. S. Perdigao, J. M. Alonso, M. A. Dalla Costa, and E. S. Saraiva, "A variable inductor MATLAB/Simulink behavioral model for application in magnetically-controlled electronic ballasts," in *Proc. Int. Symp. Power Electron. Electr. Drives, Autom. Motion*, Jun. 11–13, 2008, pp. 349–354.
[16] M. S. Perdigao, "Research and development on new control techniques for electronic ballasts based on magnetic regulators," Ph.D. dissertation, Univ. Coimbra, Coimbra, Portugal. (2011). [Online] Available: https://powersimtech.com/support/resources/tutorials/define-saturable-core/
[17] "Tutorial on how to define the saturable core element," *PSIM Software, Powersim Inc.*, Rockville, MD, USA, July 2006.
[18] J. M. Alonso, M. A. Dalla Costa, M. Rico-Secades, J. Cardesín, and J. Garcia, "Investigation of a new control strategy for electronic ballasts based on variable inductor," *IEEE Trans. Ind. Electron.*, vol. 55, no. 1, pp. 3–10, Jan. 2008.
[19] J. M. Alonso, M. S. Perdigao, D. Gacio, L. Campa, and E. S. Saraiva, "Magnetic control of DC-DC resonant converters provides constant frequency operation," *Electron. Lett.*, vol. 46, no. 6, pp. 440–442, 2010.
[20] J. M. Alonso, M. S. Perdigão, D. G. Vaquero, A. J. Calleja, and E. S. Saraiva, "Analysis, design, and experimentation on constant-frequency dc-dc resonant converters with magnetic control," *IEEE Trans. Power Electron.*, vol. 27, no. 3, pp. 1369–1382, Mar. 2012.
[21] M. S. Perdigao, J. M. Alonso, M. A. Dalla Costa, and E. S. Saraiva, "Comparative analysis and experiments of resonant tanks for magnetically controlled electronic ballasts," *IEEE Trans. Ind. Electron.*, vol. 55, no. 9, pp. 3201–3211, Sep. 2008.
[22] M. S. Perdigao, J. P. F. Trovao, J. M. Alonso, and E. S. Saraiva, "Large-signal characterization of power inductors in EV bidirectional DC–DC converters focused on core size optimization," *IEEE Trans. Ind. Electron.*, vol. 62, no. 5, pp. 3042–3051, May 2015.
[23] M. S. Perdigao, J. M. Alonso, and E. S. Saraiva, "Magnetically-controlled dimming technique with isolated output," *Electron. Lett.*, vol. 45, no. 14, pp. 756–758, Jul. 2009.
[24] M. S. Perdigao, J. M. Alonso, M. A. Dalla Costa, and E. S. Saraiva, "Using magnetic regulators for the optimization of universal ballasts," *IEEE Trans. Power Electron.*, vol. 23, no. 6, pp. 3126–3134, Nov. 2008.
[25] M. S. Perdigao, M. Menke, A. R. Seidel, R. A. Pinto, and J. M. Alonso, "A review on variable inductors and variable transformers: Applications to lighting drivers," *IEEE Trans. Ind. Appl.*, vol. 52, no. 1, pp. 531–547, Sep. 2015.
[26] R. A. Alonso, J. M. Perdigao M. S. Pinto, M. F. da Silva, and R. N. do Prado, "A new technique to equalize branch currents in multiarray LED lamps based on variable inductor," in *Proc. IEEE Ind. Appl. Soc.*, Oct. 5–9, 2014, pp. 1–9.
[27] J. M. Alonso, G. Martínez, M. Perdigão, M. Cosetin, and R. N. do Prado, "Modeling magnetic devices using spice: application to variable inductors," in *Proc. IEEE Appl. Power Electron. Conf.*, Long Beach, CA, USA, Mar. 2016, pp. 20–24.
[28] J. R. Brauer, "Simple equations for the magnetization and reluctivity curves of steel," *IEEE Trans. Magn.*, vol. 11, no. 1, p. 81, Jan 1975.
[29] T. Hülsmann, "Nonlinear material curve modeling and sensitivity analysis for MQS-problems," M.S. thesis, Faculty Elect., Inf. Media Eng., Bergische Universitat Wuppertal, Wuppertal, Germany, 2012.
[30] Ferrite Cores and Accessories Datasheet, *EPCOS*, Munich, Germany, Sep. 2006.
[31] LTspice IV. Getting Started Guide, Linear Technology Corp., Milpitas, CA, USA, 2011.
[32] J. M. Alonso, M. Perdigão, M. A. Dalla Costa, G. Martínez, and R. Osorio, "Analysis and design of a novel variable-inductor-based LED driver for DC lighting Grids," to be published in *Proc. IEEE Ind. Appl. Soc. Annu. Meeting*, Portland, OR, USA, 2016.
[33] J. M. Alonso, M. Perdigão, G. Z. Abdelmessih, and M. A. Dalla Costa, "SPICE-aided design of a variable inductor in LED driver applications," to be published in *Proc. IEEE Ind. Appl. Soc. Annu. Meeting*, Portland, OR, USA, 2016.

J. Marcos Alonso (S'94–M'98–SM'03) received the M.Sc. and Ph.D. degrees in electrical engineering from the University of Oviedo, Oviedo, Spain, in 1990 and 1994, respectively.

Since 2007, he has been a Full Professor at the Electrical Engineering Department, the University of Oviedo. He is the coauthor of more than 350 journal and conference publications, including 85 publications in highly referenced journals. His research interests include electronic ballasts, light-emitting diode power supplies, power factor correction, dc–dc converters, soft-switching converters, resonant inverters, and high-frequency switching converters in general. He was a supervisor of nine Ph.D. thesis and he is the holder of seven Spanish patents. He has participated in more than 50 research projects and contracts with companies. He has been a Visiting Researcher at the Federal University of Santa Maria, Santa Maria, Brazil, in 2011 and 2014, and at the Center for Power Electronics Systems, Virginia Tech., Blacksburg, USA, in 2013.

Dr. Alonso received the Early Career Award of the IEEE Industrial Electronics Society in 2006, and the University of Oviedo Electrical Engineering Doctorate Award, and five IEEE paper awards. He also received the National Funding for Intensification of Research Activity 2008–2012. He is a member of the Power Electronics Technical Committee of the IEEE Industrial Electronics Society. He is also a member of the European Power Electronics Association and he belongs to the International Steering Committee of the European Conference on Power Electronics and Applications. He serves as an Associate Editor of the IEEE TRANSACTIONS ON POWER ELECTRONICS and IEEE JOURNAL ON EMERGING AND SELECTED TOPICS ON POWER ELECTRONICS. He has been Coguest Editor of three special issues on lighting applications published in IEEE journals and has co-organized many IEEE Conference Special Sessions. He was Secretary of the IEEE IAS Industrial Lighting and Display Committee for the term 2013–2014, where he currently serves as Vice-Chair. He has been elected as a Member-at-Large of the IEEE IAS Executive Board for the term 2013–2016, where he collaborates in the Education department and is the Editor of the monthly IAS Newsletter.

Gilberto Martínez received the B.Sc. and M.Sc. degrees in electronic engineering from the Technology Institute of Celaya, Guanajuato, Mexico, in 2007 and 2010, respectively. Since September 2014, he has been working toward the Ph.D. degree in electrical and electronics engineering at the University of Oviedo, Oviedo, Spain.

He was with Philips Lighting as a Design Engineer of fluorescent, LED, and high-intensity discharge Lamp Drivers from December 2010 to April 2014. In July 2014, he joined R&D Continental Automotive as SMPS and LED Drivers Modules Development Engineer. His research interests include electronic ballast, dc–dc power converters, dc–dc switched capacitor converters, power converter modeling, and lighting in general.

Marina S. Perdigão (S'06–M'12) was born in Coimbra, Portugal, in 1978. She received the M.Sc. and Ph.D. degrees in electrical engineering from the University of Coimbra, Coimbra, Portugal, in 2004 and 2012, respectively. She received the Ph.D. degree from the University of Coimbra, in 2012, in cooperation with the University of Oviedo, Spain.

Since 2002, she has been with the Polytechnic Institute of Coimbra, Coimbra Institute of Engineering, Coimbra, first as a Teaching Assistant, and since 2012 as an Assistant Professor. Since 2001, she has also been a researcher at the Instituto de Telecomunicações, Coimbra. Her research interests include high-frequency electronic ballasts, discharge lamp modeling, high-frequency switching converters, resonant converters, dc–dc converters, power electronics for renewable energies, IPT and computer simulation applications. She collaborates as a transactions paper reviewer.

Dr. Perdigão received the Best Paper Award of the 2009 IEEE International Symposium on Industrial Electronics.

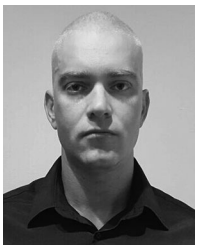

Marcelo Rafael Cosetin was born in Horizontina, Brazil, in 1985. He received the B.S. (Hons.) degree and the master's degree in electrical engineering from Federal University of Santa Maria (UFSM), Santa Maria, Brazil, in 2011 and 2013, respectively, where he is currently working toward the Ph.D. degree at Programa de Pós-Graduação em Engenharia Elétrica, concept six Capes.

In the first semester of 2011, he held Supervised Internship at Fraunhofer Institute for Reliability and Microintegration, Berlin, Germany. Since 2007, he has been a Researcher of Electronic Ballast Research Group, (UFSM. He is also a student/researcher for one year at University of Oviedo, Oviedo, Spain, at the research group Conversión Eficiente de Energía, Electrónica Industrial e Iluminación CE3I2, Gijón, supported by Science Without Boarding Brazilian Mobility Program, Capes/Cnpq. His main areas of interest includes intelligent lighting, electronics ballast, dc/dc converters, power factor correction stages, dimming systems, light-emitting-diode as lighting source, resonant ballast, and variable inductor.

Ricardo N. do Prado (M'00) received the B.Sc. degree in electrical engineering from the Federal University of Santa Maria, Santa Maria, Brazil, in 1984, and the M.Sc. and Ph.D. degrees in electrical engineering from the Federal University of Santa Catarina, Florianopolis, Brazil, in 1987 and 1993, respectively.

From 1987 to 1992, he was with the Federal University of Minas Gerais, Belo Horizonte, Brazil. Since 1993, he has been with the Federal University of Santa Maria, where he is currently a Full Professor with the Department of Electrical Energy Processing. From 2005 to 2006, he was a Postdoctoral Research Scholar with the Fraunhofer Institute, Munich, Germany. He is the author of more than 250 technical papers published in conference proceedings and magazines. He was a Co-Guest Editor of the Special Issue on Power Electronics Applications to Lighting Systems published in the *Power Electronics Brazilian Journal* (2012/2013), and he has co-organized several conference special sessions. His research interests include high frequency, fluorescent, and high-pressure lamps, dimming systems, luminous efficiency, electronic ballast, light emitting diode as a source light, and power-factor correction.

Dr. Prado is a founding member of the Brazilian Power Electronics Society and a member of the Brazilian Automatic Control Society and several IEEE societies. He is a Reviewer for the Brazilian Power Electronics Society, Brazilian Automatic Control Society, and several IEEE Societies. He received one IEEE paper awards.